MATCHED DIRECTION DETECTORS

Olivier Besson[†], *Louis L. Scharf*[*] *and François Vincent*[†]

[†]Department of Avionics and Systems, ENSICA, Toulouse, France.
[*]Departments of ECE and Statistics, Colorado State University, Fort Collins, USA.

ABSTRACT

In this paper, we address the problem of detecting a signal whose associated spatial signature is subject to uncertainties, in the presence of subspace interference and broadband noise, and using multiple snapshots from an array of sensors. To account for steering vector uncertainties, we assume that the spatial signature of interest lies in a given linear subspace $\langle \boldsymbol{H} \rangle$ while its coordinates in this subspace are unknown. The generalized likelihood ratio test (GLRT) for the problem at hand is formulated. We show that the GLRT amounts to searching for the best direction in the subspace $\langle \boldsymbol{H} \rangle$ after projecting out the interferences. The distribution of the GRLT under both hypotheses is derived and numerical simulations illustrate its performance.

1. PROBLEM FORMULATION

An ubiquitous task in many applications of radar, sonar or communications consists in detecting the presence of and recovering a signal of interest in the presence of interferences and noise using an array of L sensors [1]. In most cases, the spatial (or space-time) signature of interest $\boldsymbol{a}$ is assumed to be known. However, exact knowledge of $\boldsymbol{a}$ is a rather idealistic assumption since many factors can possibly give rise to uncertainties about $\boldsymbol{a}$. These include uncalibrated arrays, uncertainties about the direction of arrival (DOA) of the source, local scattering, etc. Whenever the actual signature differs from the presumed one, and unless some proper measures are taken, performance degradation is observed. In order to account for these mismatches, we assume that the steering vector of interest belongs to a known linear subspace $\langle \boldsymbol{H} \rangle$ but that its coordinates within this subspace are otherwise unknown. To motivate this type of modelling, let us consider the case of a Ricean channel for which the steering vector can be written as

$$\boldsymbol{a} = \boldsymbol{a}_0 + \frac{1}{\sqrt{q}} \sum_{k=1}^{q} g_k \boldsymbol{a}(\theta_k) \tag{1}$$

where $\boldsymbol{a}_0$ corresponds to the line-of-sight component. The g_k are zero-mean, independent and identically distributed random variables with power σ_g^2, and θ_k are independent random variables with probability density function $p(\theta)$. The covariance matrix of the steering vector errors is then $\boldsymbol{C}_a = \sigma_g^2 \int \boldsymbol{a}(\theta)\boldsymbol{a}^H(\theta)p(\theta)\, d\theta$. When the standard deviation of θ_k (referred to as angular spread in the literature) is small, it is well-known that the covariance matrix of the Slepian matrix $\boldsymbol{C}_a$ is close to rank-deficient. Therefore, one can define an "effective rank" r that contains most of the energy in the eigenvalues of $\boldsymbol{C}_a$. That is, $\boldsymbol{C}_a \simeq \boldsymbol{U}_r \boldsymbol{\Lambda}_r \boldsymbol{U}_r^H$ where $\boldsymbol{U}_r$ contains the r dominant eigenvectors and $\boldsymbol{\Lambda}_r$ is the diagonal matrix of the r dominant eigenvalues. Consequently the actual steering vector approximately lies in the subspace spanned by $\begin{bmatrix}\boldsymbol{a}_0 & \boldsymbol{U}_r\end{bmatrix}$. A subspace approach to model spatial signatures in the presence of local scattering is also advocated in [2] where it is referred to as a generalized array manifold. This modelling is also relevant in space-time problems to account for straddling, i.e. when the presence of a target is detected on a grid of potential spatial and Doppler frequencies whereas the actual spatial and Doppler frequencies lie in between the grid [3]. See also [4] where the space-time steering vector is modelled as the rank-one Kronecker product of a spatial and a temporal signature, each subject to uncertainties and assumed to belong to a linear subspace. Therefore, the overall space-time signature belongs to some subspace.

Hereafter, we thus consider the following model for the L-dimensional received signal

$$\begin{aligned} &\boldsymbol{y}(t) = \boldsymbol{x}(t) + \boldsymbol{i}(t) + \boldsymbol{n}(t); \quad t = 1, \cdots, N \\ &\boldsymbol{x}(t) = \boldsymbol{a}s(t); \quad \boldsymbol{i}(t) = \boldsymbol{A}\boldsymbol{u}(t) \end{aligned} \tag{2}$$

where $\boldsymbol{a} = \boldsymbol{H}\boldsymbol{\theta}$ is the steering vector of interest which belongs to the p-dimensional subspace $\langle \boldsymbol{H} \rangle$ and $s(t)$ is the emitted signal waveform. In (2) $\boldsymbol{A}$ stands for the J-dimensional interference subspace and $\boldsymbol{u}(t)$ denotes the interferences waveforms. Finally, $\boldsymbol{n}(t)$ is a zero-mean complex-valued Gaussian noise with covariance matrix $\sigma^2\boldsymbol{I}$. In this paper we assume that $\boldsymbol{H}$ and $\boldsymbol{A}$ are known full-rank matrices, and that the subspaces $\langle \boldsymbol{H} \rangle$ and $\langle \boldsymbol{A} \rangle$ are linearly independent. Furthermore, we consider the case where $J + p < L$. Moreover, it is assumed that $s(t)$ and $\boldsymbol{u}(t)$ are deterministic sequences such that

$$\lim_{N\to\infty} \frac{1}{N} \sum_{t=1}^{N} \begin{bmatrix} s(t) \\ \boldsymbol{u}(t) \end{bmatrix} \begin{bmatrix} s^*(t) & \boldsymbol{u}^H(t) \end{bmatrix} = \begin{bmatrix} P & \boldsymbol{0}^H \\ \boldsymbol{0} & \boldsymbol{\Pi} \end{bmatrix} \tag{3}$$

where $\boldsymbol{\Pi}$ is a full-rank matrix. Finally, we assume that the noise level σ^2 is known. Since there exists an inherent scaling ambiguity between $\boldsymbol{\theta}$ and $s(t)$ in (2), a constraint may be enforced on $\boldsymbol{\theta}$. A meaningful constraint, when the first column of $\boldsymbol{H}$ is $\boldsymbol{a}_0$, is to set the first element of $\boldsymbol{\theta}$ to 1. This is the convention we adopt in the sequel.

The problem we consider herein is to decide for the presence of the component $\boldsymbol{x}(t)$, having observed N snapshots $\{\boldsymbol{y}(t)\}_{t=1}^N$. It is worth pointing out at this stage that the problem considered here is related to that in [1, 5]. However, the model in (2) considers multiple snapshots and shows a major difference with that of [1, 5]. The model in [1, 5] for multiple snapshots would be $\boldsymbol{y}(t) = \boldsymbol{H}\boldsymbol{s}(t) + \boldsymbol{A}\boldsymbol{u}(t) + \boldsymbol{n}(t)$ with $\boldsymbol{s}(t)$ a $p \times 1$ vector, whereas the model herein writes $\boldsymbol{y}(t) = \boldsymbol{H}\boldsymbol{\theta}s(t) + \boldsymbol{A}\boldsymbol{u}(t) + \boldsymbol{n}(t)$, with

The work of L.L. Scharf is supported by the Office of Naval Research under Contract N00014-01-1-1019.

$\boldsymbol{s}(t)$ forced to be $\boldsymbol{\theta}s(t)$. Hence, the problems are different, as will be the associated estimators. However, for $N = 1$ the problems become identical and we will show later that the GLRT derived here reduces to that of [5] in the single-snapshot case. We will further elaborate on this aspect after the derivation of the GLRT.

2. GENERALIZED LIKELIHOOD RATIO TEST

Our problem can thus be recast as that of deciding between the two hypotheses

$$\begin{cases} H_0: & \mu = 0 \\ H_1: & \mu = 1 \end{cases} \tag{4}$$

in the model

$$\boldsymbol{Y} = \mu \boldsymbol{H}\boldsymbol{\theta}\boldsymbol{s}^T + \boldsymbol{A}\boldsymbol{U} + \boldsymbol{N} \tag{5}$$

where $\boldsymbol{Y} = \begin{bmatrix}\boldsymbol{y}(1) & \cdots & \boldsymbol{y}(N)\end{bmatrix}$, $\boldsymbol{s} = \begin{bmatrix}s(1) & \cdots & s(N)\end{bmatrix}$ and $\boldsymbol{U} = \begin{bmatrix}\boldsymbol{u}(1) & \cdots & \boldsymbol{u}(N)\end{bmatrix}$. In order to derive the GLRT, the maximum likelihood estimator (MLE) must be obtained as a first step. Towards this end, observe that the observations are proper Gaussian distributed so that the likelihood function is given by [1]

$$\ell(\boldsymbol{Y}) = \left(\pi\sigma^2\right)^{-mN} e^{-\frac{1}{\sigma^2}\sum_{t=1}^{N}\|\boldsymbol{y}(t)-\mu\boldsymbol{H}\boldsymbol{\theta}s(t)-\boldsymbol{A}\boldsymbol{u}(t)\|^2}. \tag{6}$$

The MLE amounts to maximizing $\ell(\boldsymbol{Y})$ or equivalently minimizing

$$\begin{aligned}\Lambda &= \sum_{t=1}^{N}\|\boldsymbol{y}(t) - \mu\boldsymbol{H}\boldsymbol{\theta}s(t) - \boldsymbol{A}\boldsymbol{u}(t)\|^2 \\ &= \mathrm{Tr}\left\{\left(\boldsymbol{Y} - \mu\boldsymbol{H}\boldsymbol{\theta}\boldsymbol{s}^T - \boldsymbol{A}\boldsymbol{U}\right)\left(\boldsymbol{Y} - \mu\boldsymbol{H}\boldsymbol{\theta}\boldsymbol{s}^T - \boldsymbol{A}\boldsymbol{U}\right)^H\right\}\end{aligned} \tag{7}$$

with respect to (w.r.t.) $\boldsymbol{s}, \boldsymbol{U}$ and $\boldsymbol{\theta}$. For any given $\boldsymbol{s}$ and $\boldsymbol{\theta}$, the matrix $\boldsymbol{U}$ which minimizes (7) is given by [1]

$$\boldsymbol{U} = \left(\boldsymbol{A}^H\boldsymbol{A}\right)^{-1}\boldsymbol{A}^H\left(\boldsymbol{Y} - \mu\boldsymbol{H}\boldsymbol{\theta}\boldsymbol{s}^T\right). \tag{8}$$

Under hypothesis H_0, $\boldsymbol{U}$ is the only unknown component and the estimation procedure ends with (8). Under H_1, $\boldsymbol{s}$ and $\boldsymbol{\theta}$ are still to be determined. To obtain them, let us report (8) in (7) which yields the problem of minimizing

$$\begin{aligned}\widehat{\Lambda} &= \mathrm{Tr}\left\{\left(\boldsymbol{Y} - \boldsymbol{H}\boldsymbol{\theta}\boldsymbol{s}^T\right)^H\boldsymbol{P}_{\boldsymbol{A}}^{\perp}\left(\boldsymbol{Y} - \boldsymbol{H}\boldsymbol{\theta}\boldsymbol{s}^T\right)\right\} \\ &= \left(\boldsymbol{\theta}^H\boldsymbol{H}^H\boldsymbol{P}_{\boldsymbol{A}}^{\perp}\boldsymbol{H}\boldsymbol{\theta}\right)\left\|\boldsymbol{s}^* - \frac{\boldsymbol{Y}^H\boldsymbol{P}_{\boldsymbol{A}}^{\perp}\boldsymbol{H}\boldsymbol{\theta}}{\boldsymbol{\theta}^H\boldsymbol{H}^H\boldsymbol{P}_{\boldsymbol{A}}^{\perp}\boldsymbol{H}\boldsymbol{\theta}}\right\|^2 \\ &\quad + \mathrm{Tr}\left\{\boldsymbol{P}_{\boldsymbol{A}}^{\perp}\boldsymbol{Y}\boldsymbol{Y}^H\right\} - \frac{\boldsymbol{\theta}^H\boldsymbol{H}^H\boldsymbol{P}_{\boldsymbol{A}}^{\perp}\boldsymbol{Y}\boldsymbol{Y}^H\boldsymbol{P}_{\boldsymbol{A}}^{\perp}\boldsymbol{H}\boldsymbol{\theta}}{\boldsymbol{\theta}^H\boldsymbol{H}^H\boldsymbol{P}_{\boldsymbol{A}}^{\perp}\boldsymbol{H}\boldsymbol{\theta}}\end{aligned} \tag{9}$$

where $\boldsymbol{P}_{\boldsymbol{A}}$ denotes the orthogonal projection onto $\langle\boldsymbol{A}\rangle$ and $\boldsymbol{P}_{\boldsymbol{A}}^{\perp} = \boldsymbol{I} - \boldsymbol{P}_{\boldsymbol{A}}$ the projection onto its orthogonal complement. Note that $\boldsymbol{P}_{\boldsymbol{A}}^{\perp}\boldsymbol{H} \neq \boldsymbol{0}$ under the hypotheses made. The maximum likelihood estimate of $\boldsymbol{\theta}$ is thus given, up to a scaling factor, by the principal generalized eigenvector of $\left(\boldsymbol{G}^H\widehat{\boldsymbol{R}}\boldsymbol{G}, \boldsymbol{G}^H\boldsymbol{G}\right)$ with $\boldsymbol{G} = \boldsymbol{P}_{\boldsymbol{A}}^{\perp}\boldsymbol{H}$ and

$$\widehat{\boldsymbol{R}} = N^{-1}\boldsymbol{Y}\boldsymbol{Y}^H. \tag{10}$$

$\widehat{\boldsymbol{R}}$ is the sample covariance matrix. In other words

$$\widehat{\boldsymbol{\theta}} = \beta\mathcal{P}\left\{\left(\boldsymbol{G}^H\boldsymbol{G}\right)^{-1}\boldsymbol{G}^H\widehat{\boldsymbol{R}}\boldsymbol{G}\right\} \tag{11}$$

where $\mathcal{P}\{.\}$ stands for the principal eigenvector of the matrix between braces, and the scalar β is determined such that $\widehat{\theta}_1 = 1$. This result shows that, when multiple snapshots are available, a preferred direction in the subspace $\langle\boldsymbol{G}\rangle$ may be determined. When $\boldsymbol{A} = \boldsymbol{0}$, the preferred direction in $\langle\boldsymbol{H}\rangle$ is $\mathcal{P}\left\{\boldsymbol{P}_{\boldsymbol{H}}\widehat{\boldsymbol{R}}\right\}$ where $\boldsymbol{P}_{\boldsymbol{H}}$ denotes the orthogonal projection onto $\langle\boldsymbol{H}\rangle$.

The (logarithmic) GLR is given by

$$L_1(\boldsymbol{Y}) = \ln\frac{\widehat{\ell}(\boldsymbol{Y}|H_1)}{\widehat{\ell}(\boldsymbol{Y}|H_0)} = \frac{1}{\sigma^2}\left[\left\|\widehat{\boldsymbol{N}}_0\right\|^2 - \left\|\widehat{\boldsymbol{N}}_1\right\|^2\right] \tag{12}$$

where $\widehat{\ell}(\boldsymbol{Y}|H_k)$ is the likelihood function under hypothesis k with the unknown parameters replaced by their ML estimates. $\widehat{\boldsymbol{N}}_0$ and $\widehat{\boldsymbol{N}}_1$ are the ML estimates of $\boldsymbol{N}$ under H_0 and H_1 respectively. Using (9), we have

$$\left\|\widehat{\boldsymbol{N}}_0\right\|^2 = \mathrm{Tr}\left\{\boldsymbol{P}_{\boldsymbol{A}}^{\perp}\boldsymbol{Y}\boldsymbol{Y}^H\right\} \tag{13}$$

$$\left\|\widehat{\boldsymbol{N}}_1\right\|^2 = \mathrm{Tr}\left\{\boldsymbol{P}_{\boldsymbol{A}}^{\perp}\boldsymbol{Y}\boldsymbol{Y}^H\right\} - \lambda_{\max}\left\{\boldsymbol{P}_{\boldsymbol{G}}\boldsymbol{Y}\boldsymbol{Y}^H\right\} \tag{14}$$

where $\lambda_{\max}\{.\}$ is the largest eigenvalue of the matrix between braces. It follows that the GLRT takes the following form

$$L_1(\boldsymbol{Y}) = \frac{1}{\sigma^2}\lambda_{\max}\left\{\boldsymbol{P}_{\boldsymbol{G}}\boldsymbol{Y}\boldsymbol{Y}^H\right\} \lessgtr \eta. \tag{15}$$

Briefly stated, the detector consists of searching for the *direction of maximum energy* in the subspace $\langle\boldsymbol{G}\rangle$, i.e. in the part of $\langle\boldsymbol{H}\rangle$ which is orthogonal to the interference subspace. Equivalently, it computes the covariance of $\boldsymbol{Y}$ in the subspace $\langle\boldsymbol{G}\rangle$ and tests the energy along its principal direction. Hence, the detector here can be called a *matched direction detector*. This contrasts with the corresponding detector in [5] which would use $\mathrm{Tr}\left\{\boldsymbol{P}_{\boldsymbol{G}}\boldsymbol{Y}\boldsymbol{Y}^H\right\}$, the total energy in $\langle\boldsymbol{G}\rangle$, as the signal would be allowed to move around in the subspace $\langle\boldsymbol{H}\rangle$ from snapshot to snapshot. In the present paper, the signal is fixed in the subspace $\langle\boldsymbol{H}\rangle$ and multiple snapshots may be used to estimate its fixed location $\boldsymbol{H}\widehat{\boldsymbol{\theta}}$. Therefore, the detector searches for a single vector in $\langle\boldsymbol{G}\rangle$, namely the one which bears most energy, and then compares this energy to a threshold. This is illustrated in Figure 1 in the simplest case of no interference. When multiple snapshots (represented by the arrows) are available, the detector in [5] would project them anywhere in $\langle\boldsymbol{H}\rangle$ (the circles) with no additional constraint while the rank-one model here imposes that they lie along one direction (the squares).

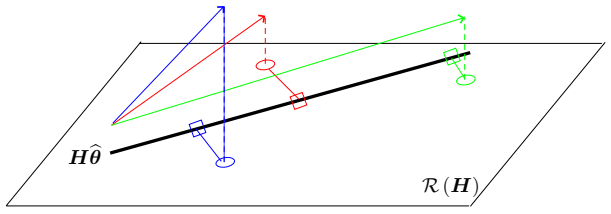

Fig. 1. Differences between the matched subspace detector and the matched direction detector.

In order to set the threshold η of the test for a given probability of false alarm P_{FA} and to obtain the probability of detection, it is required to derive the probability density function (PDF) of $\sigma^{-2}\lambda_{\max}\left\{\boldsymbol{P}_{\boldsymbol{G}}\boldsymbol{Y}\boldsymbol{Y}^H\right\}$ or at least its cumulative distribution

function (CDF). For notational convenience, let us define $s = \min(p, N)$, $t = \max(p, N)$ and let us denote by ϕ_s the largest eigenvalue of $\sigma^{-2}\boldsymbol{P_G}\boldsymbol{Y}\boldsymbol{Y}^H$. Also, let $\boldsymbol{U}_G \in \mathbb{C}^{L\times p}$ be a unitary basis for $\langle \boldsymbol{G} \rangle$. Under the null hypothesis

$$\begin{aligned} L_1(\boldsymbol{Y}|H_0) &= \sigma^{-2}\lambda_{\max}\left\{\boldsymbol{P_G}\boldsymbol{Y}\boldsymbol{Y}^H\right\} \\ &= \sigma^{-2}\lambda_{\max}\left\{\boldsymbol{P_G}\left[\boldsymbol{A}\boldsymbol{U}+\boldsymbol{N}\right]\left[\boldsymbol{A}\boldsymbol{U}+\boldsymbol{N}\right]^H\right\} \\ &= \lambda_{\max}\left\{\sigma^{-2}\boldsymbol{P_G}\boldsymbol{N}\boldsymbol{N}^H\right\} = \lambda_{\max}\left\{\sigma^{-2}\boldsymbol{U}_G\boldsymbol{U}_G^H\boldsymbol{N}\boldsymbol{N}^H\right\} \\ &= \lambda_{\max}\left\{\sigma^{-2}\boldsymbol{U}_G^H\boldsymbol{N}\boldsymbol{N}^H\boldsymbol{U}_G\right\} \\ &= \lambda_{\max}\left\{\sigma^{-2}\widetilde{\boldsymbol{N}}\widetilde{\boldsymbol{N}}^H\right\} \end{aligned} \tag{16}$$

where $\widetilde{\boldsymbol{N}} = \boldsymbol{U}_G^H\boldsymbol{N}$ is a $p\times N$ matrix whose columns are independent p-variate complex Gaussian vectors with covariance matrix $\sigma^2\boldsymbol{I}$. Then, the CDF of ϕ_s is given by [6]

$$\Pr\left(\phi_s \le \eta|H_0\right) = \frac{|\boldsymbol{\Psi}_c(\eta)|}{\prod_{k=1}^{s}\Gamma(t-k+1)\Gamma(s-k+1)} \tag{17}$$

where $\boldsymbol{\Psi}_c(\eta)$ is an $s\times s$ Hankel matrix function of $\eta \ge 0$ whose (k,ℓ) element is given by

$$\left[\boldsymbol{\Psi}_c(\eta)\right]_{k,\ell} = \gamma(t-s+k+\ell-1,\eta) \tag{18}$$

and $\gamma(n,x) = \int_0^x t^{n-1}e^{-t}\,dt$ stands for the incomplete gamma function. Equation (17) provides the necessary material to compute the threshold η for a given $P_{\text{FA}} = 1 - \Pr\left(\phi_s \le \eta|H_0\right)$.

Under H_1, the GLR can be written as

$$\begin{aligned} L_1(\boldsymbol{Y}|H_1) &= \lambda_{\max}\left\{\sigma^{-2}\boldsymbol{P_G}\left[\boldsymbol{a}\boldsymbol{s}^T+\boldsymbol{N}\right]\left[\boldsymbol{a}\boldsymbol{s}^T+\boldsymbol{N}\right]^H\right\} \\ &= \lambda_{\max}\left\{\sigma^{-2}\boldsymbol{U}_G^H\left[\boldsymbol{a}\boldsymbol{s}^T+\boldsymbol{N}\right]\left[\boldsymbol{a}\boldsymbol{s}^T+\boldsymbol{N}\right]^H\boldsymbol{U}_G\right\} \\ &= \lambda_{\max}\left\{\sigma^{-2}\widetilde{\boldsymbol{Y}}\widetilde{\boldsymbol{Y}}^H\right\} \end{aligned} \tag{19}$$

with $\widetilde{\boldsymbol{Y}} = \boldsymbol{U}_G^H\left[\boldsymbol{a}\boldsymbol{s}^T+\boldsymbol{N}\right]$. Hence, $\widetilde{\boldsymbol{Y}}$ has a multivariate normal distribution with mean $\boldsymbol{M} = \boldsymbol{U}_G^H\boldsymbol{a}\boldsymbol{s}^T$ and covariance matrix $\sigma^2\boldsymbol{I}$. The results of [6] -especially Corollary 1 and Appendix B- can again be used to obtain the PDF or CDF of $L_1(\boldsymbol{Y}|H_1)$. More precisely, let $\lambda_1 = \sigma^{-2}\left\|\boldsymbol{U}_G^H\boldsymbol{a}\right\|^2\|\boldsymbol{s}\|^2$ be the single nonzero eigenvalue of $\sigma^{-2}\boldsymbol{M}^H\boldsymbol{M}$. Then, the CDF of $L_1(\boldsymbol{Y}|H_1)$ is given by [6]

$$\Pr\left(\phi_s \le \eta|H_1\right) = \frac{e^{-\lambda_1}}{\Gamma(t-s+1)\lambda_1^{s-1}}\frac{|\boldsymbol{\Psi}_{\text{i.i.d}}(\eta)|}{\prod_{k=1}^{s-1}\Gamma(t-k)\Gamma(s-k)} \tag{20}$$

where $\boldsymbol{\Psi}_{\text{i.i.d}}(\eta)$ is a $s\times s$ matrix whose expression can be found in [6]. Equation (20) enables us to calculate the probability of detection, $P_{\text{D}} = 1 - \Pr\left(\phi_s \le \eta|H_1\right)$.

3. NUMERICAL ILLUSTRATIONS

In this section, we illustrate the performance of the GLRT detector. Throughout this section, we consider a uniform linear array of $L = 10$ sensors spaced a half-wavelength apart. The source of interest impinges from broadside and we consider the case of a Ricean channel. We assume a Gaussian distribution for the scatterers with standard deviation $\sigma_\theta = 15^\circ$. The actual steering vector is generated as

$$\boldsymbol{a} = \boldsymbol{a}_0 + \boldsymbol{U}_r\boldsymbol{\Lambda}_r^{1/2}\boldsymbol{\theta}_2 = \boldsymbol{a}_0 + \boldsymbol{H}_2\,\boldsymbol{\theta}_2 \tag{21}$$

where $\boldsymbol{U}_r$ is the matrix formed by the r principal eigenvectors of $\boldsymbol{C}_a$. Unless otherwise stated, $r = 2$ and $\boldsymbol{\theta}_2$ is drawn from a proper complex-valued multivariate normal distribution with zero-mean and unit variance. We define the uncertainty ratio (UR) as

$$UR = 10\log_{10}\left(\frac{\text{Tr}\left\{\boldsymbol{H}_2^H\boldsymbol{H}_2\right\}}{\boldsymbol{a}_0^H\boldsymbol{a}_0}\right). \tag{22}$$

UR as defined above measures the ratio of the average power of the non-line of sight component to the power of the line of sight component. In all simulations, we consider that the noise component consists of a proper complex white noise contribution with power σ^2 and two interferences whose DOAs are -20°, 30° and whose powers are 20dB and 30dB above the white noise level, respectively. The signal to noise ratio (SNR) is defined as

$$SNR = 10\log_{10}\left(\frac{P\left[\boldsymbol{a}_0^H\boldsymbol{a}_0 + \text{Tr}\left\{\boldsymbol{H}_2^H\boldsymbol{H}_2\right\}\right]}{\sigma^2}\right).$$

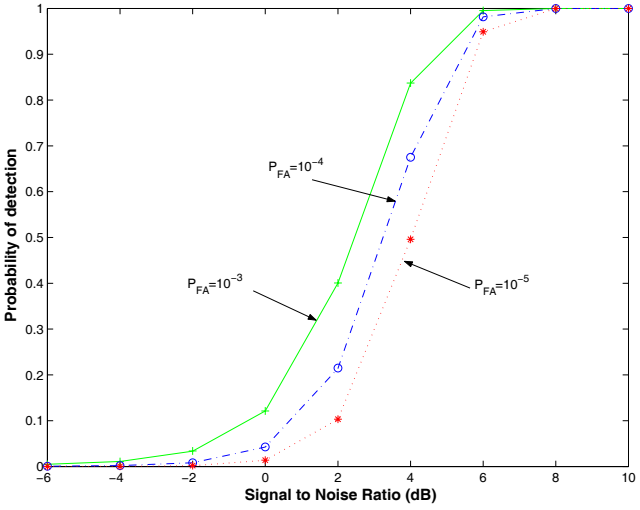

Fig. 2. Theoretical and empirical probability of detection versus SNR. $UR = -6$dB and $N = 10$.

First, we validate the theoretical expression of P_{D} as given by (20). Towards this end, a fixed $\boldsymbol{a}$ is drawn from (21) and 500 000 simulations are run to evaluate the empirical probability of detection. The latter is compared with the theoretical probability of detection in Figure 2. As can be observed the empirical and theoretical results are in perfect agreement, which validates (20).

Next, we characterize the average behavior of the GLRT by changing $\boldsymbol{a}$ in each of the 500 000 runs. Figure 3 displays the average probability of detection versus the SNR for different P_{FA}. Comparing Figures 2 and 3 it follows that the "average" behavior is similar to that obtained with a single realization of $\boldsymbol{a}$. In Figure 4 we investigate the influence of the number of snapshots N on the detection performance. The false alarm probability is set to

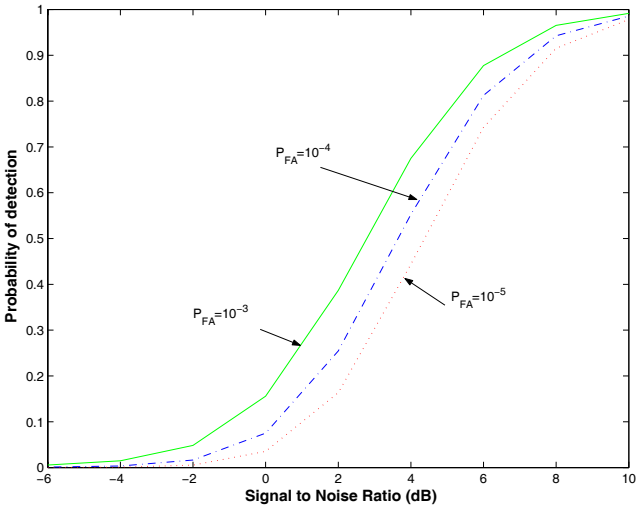

Fig. 3. Average probability of detection versus SNR. $UR = -6$dB and $N = 10$.

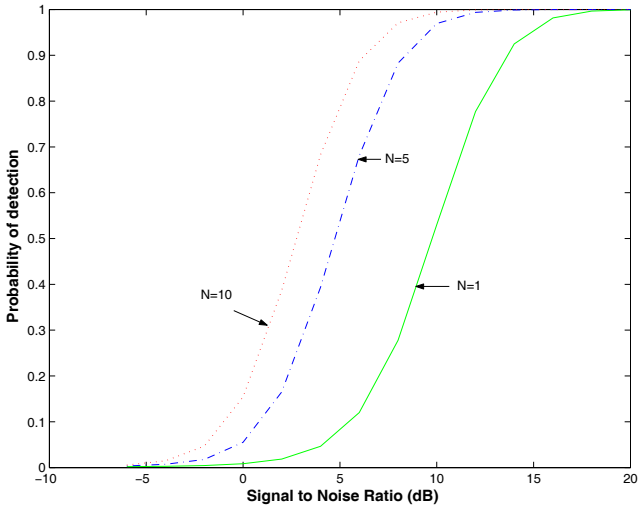

Fig. 4. Average probability of detection versus SNR for various number of snapshots. $P_{\text{FA}} = 10^{-3}$ and $UR = -6$dB.

$P_{\text{FA}} = 10^{-3}$. It can be observed that N has a significant influence on the detection performance, especially in moderate SNR where P_{D} can be significantly improved. For instance, for $P_{\text{D}} = 0.9$, a 5.4 dB SNR improvement is observed when N goes from $N = 1$ to $N = 5$, an additional 2.1 dB improvement occurs from $N = 5$ to $N = 10$.

Finally, we test the robustness of the detector when $\boldsymbol{a}$ is no longer exactly in a subspace but is generated according to (1). Figure 5 displays P_{D} for different values of the subspace's dimension. It can be observed that the best results are obtained with $p = 2$, and that no real improvement is achieved when increasing p. Note however that $\boldsymbol{a}_0$ is always included in $\langle \boldsymbol{H} \rangle$. Also, the optimal value of p depends on both the uncertainty ratio and the eigenvalue spread of $\boldsymbol{C}_a$. In conclusion, for detection purposes, subspace modelling of the spatial signature seems to be a robust and effective solution.

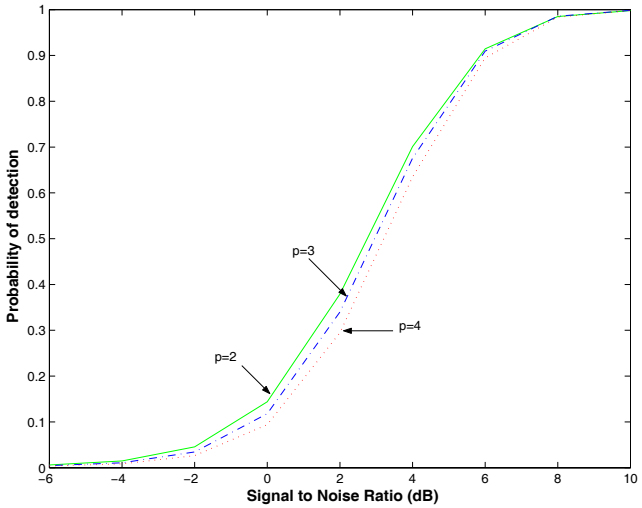

Fig. 5. Average probability of detection versus SNR for various steering vector subspace's dimension. $P_{\text{FA}} = 10^{-3}$, $UR = -6$dB and $N = 10$.

4. CONCLUSIONS

In this paper, we have considered the problem of detecting a signal whose spatial signature lies in a given linear subspace. This work can be viewed as an extension of the matched subspace detectors of [5] to the case of multiple snapshots. The main difference is that the present detector looks for a preferred direction in a subspace and computes energy along this direction instead of the energy in the whole subspace.

5. REFERENCES

[1] L.L. Scharf, *Statistical Signal Processing: Detection, Estimation and Time Series Analysis*, Addison Wesley, Reading, MA, 1991.

[2] D. Astély, B. Ottersten, and A.L. Swindlehurst, "Generalised array manifold model for wireless communication channels with local scattering," *Proceedings IEE-F Radar, Sonar Navigation*, vol. 145, no. 1, pp. 51–57, February 1998.

[3] A. Zeira and B. Friedlander, "Robust subspace detectors," in *Proceedings 31st Asilomar Conference Signals Systems Computers*, Pacific Grove, CA, November 2-5 1997, pp. 778–782.

[4] S. Bose and A.O. Steinhardt, "Adaptive array detection of uncertain rank one waveforms," *IEEE Transactions Signal Processing*, vol. 44, no. 11, pp. 2801–2809, November 1996.

[5] L.L. Scharf and B. Friedlander, "Matched subspace detectors," *IEEE Transactions Signal Processing*, vol. 42, no. 8, pp. 2146–2157, August 1994.

[6] M. Kang and M.-S. Alouini, "Largest eigenvalue of complex Wishart matrices and performance analysis of MIMO MRC systems," *IEEE Journal Selected Areas Communications*, vol. 21, no. 3, pp. 418–426, April 2003.